Met. Mater. Int., Vol. 21, No. 5 (2015), pp. 850~856
doi: 10.1007/s12540-015-5176-1

Estimation of Principal Directions of Bi-Axial Residual Stress Using Instrumented Knoop Indentation Testing

Young-Cheon Kim[1], Min-Jae Choi[2], Dongil Kwon[3], and Ju-Young Kim[1,4,*]

[1]School of Materials Science and Engineering, UNIST (Ulsan National Institute of Science and Technology), Ulsan 689-798, Korea
[2]Nuclear Materials Division, KAERI (Korea Atomic Energy Research Institute), Daejeon 305-353 Korea
[3]Department of Materials Science and Engineering, Seoul National University, Seoul 151-744, Korea
[4]KIST-UNIST Ulsan Center for Convergent Materials, UNIST, Ulsan 689-798, Korea

(received date: 9 April 2015 / accepted date: 22 June 2015)

We propose a novel method for estimating stress directionality p and principal direction θ_p using four Knoop indentations. Indentation load-depth curves with a Knoop indenter are shifted with respect to indenter orientation to stress direction. Based on this phenomenon, we derived p and θ_p theoretically in terms of the indentation load differences between a stressed and an unstressed sample. Plastic zone beneath the Knoop indenter was theoretically estimated based on expanding cavity model for confirming separate plastic zones of four Knoop indentations. The proposed models and algorithms were verified by indentation experiments under various applied stress states that are generated using a stress-generating jig with two independent orthogonal loading axes. Estimated principal directions showed good agreement with applied principal directions. For small target area when considering in-field application, we proposed an estimation method of one load difference with other three load differences, and it was verified as feasible method with experimental results.

Keywords: indentation, residual stress, metals, deformation, surface

1. INTRODUCTION

Residual stress, which inevitably develops during manufacturing processes with plastic deformation or heat treatment, is the primary factor in the fracture and failure of materials and products. Residual stress is evaluated by two kinds of methods: destructive and non-destructive testing. Destructive methods, such as saw-cutting and hole-drilling, cannot be applied to structures in operation, such as facilities or pipelines. Non-destructive methods, namely the X-ray diffraction and curvature method, generally require large equipment or laboratory-scale machines. Instrumented indentation testing (IIT), on the other hand, is non-destructive and relatively simple, and has received significant attention for measuring mechanical response of materials [1-5]. Numerous studies have used IIT to estimate residual stress using it. Tsui *et al*. [6] and Bolshakov *et al*. [7] conducted indentation tests and finite element (FE) analysis to determine that the indentation contact area is independent of applied stress at a given load. Based on this approach, Suresh and Giannakopoulos [8] developed a theoretical model to estimate residual stress in the equibiaxial stress fields that was confirmed by Carlsson and Larsson [9,10]. Swadener *et al.* [11] developed another approach to determine residual stress using a spherical indenter.

To consider a non-equibiaxial residual stress state, Giannakopoulos [12] examined analytically and experimentally the influence of surface initial stress on instrumented sharp indentation, and Lee and Kwon [13,14] suggested a quantitative method for evaluating non-equibiaxial residual stress using the stress directionality p by modifying the influence of surface stress on the contact pressure by shear plasticity and expanding the existing equibiaxial stress model. They eliminated the pure shear-stress term in the non-equibiaxial stress state and decomposed the remained stress components into hydrostatic and deviatoric stresses. Since only the deviatoric stress influences the indentation load-depth curve, they proposed a quantitative equation that relates residual stress to indentation load difference:

$$\sigma_{res}^{x} = \frac{3}{1+p}\frac{(L_0-L_S)}{A_S} \tag{1}$$

$$\sigma_{res}^{y} = p\sigma_{res}^{x} = \frac{3p}{1+p}\frac{(L_0-L_S)}{A_S} \tag{2}$$

Here L_0-L_S is the load difference determined by analyzing the load-depth curves for the unstressed and stressed states

*Corresponding author: juyoung@unist.ac.kr

at a given depth, A_S is the contact area in the stressed state and p is the stress directionality as defined by the ratio of minor to major stress components in a given biaxial stress state. However, the stress directionality and principal direction in this work were known values, and no evaluation method with indentation was proposed. In general, residual stress is not as equi-biaxial but a biaxial stress, meaning that the magnitudes of x- and y-axis stress are different.

In this study, we performed Knoop instrumented indentation testing to estimate the principal direction and stress directionality of the residual stress, as derived using a plane stress transformation with load differeces at each Knoop indenter orientation. The proposed models were verified by comparing the applied stress on cruciform specimens using stress-generating jig and results of Knoop indentations. The stresses estimated with this new method showed good agreement with in-plane applied stress.

2. THEORETICAL MODELING

The Knoop indenter has an asymmetric shape (Fig. 1) in which the ratio of long and short diagonals of an indent is 7.11:1. Because of its asymmetry, the Knoop indenter has been used to evaluate micro hardness and for studies of a material anisotropy. Zeng *et al*. [15] analyzed the residual stress field around Knoop indentations by FE numerical calculations.

Choi *et al*. [16] tried to estimate principal directions of stressed specimens using two Knoop indentations. The orientation of a Knoop indenter to a specimen in a biaxial stress state shifts the indentation load-depth curve. When the long diagonal is perpendicular to the σ_{res}^x direction, the load L_x attains its maximum at a given depth h. While the long diagonal is perpendicular to the σ_{res}^y direction, the load L_y attains its minimum because of interactive deformation behavior. The load differences, ΔL_x and ΔL_y, among L_x, L_y and the maximum load in the indentation load-depth curve for a stress-free sample were derived analytically by considering the effect of each principal stress on the indentation load:

$$\Delta L_x = \alpha_{//}\sigma_{res}^x + \alpha_{\perp}\sigma_{res}^y \tag{3a}$$

$$\Delta L_y = \alpha_{\perp}\sigma_{res}^x + \alpha_{//}\sigma_{res}^y \tag{3b}$$

where $\alpha_{//}$ and $\alpha_{\perp}$ are the conversion factors relating the residual stress to the load difference, and their subscripts denote direction between the long diagonal and principal stress. In previous work [16], the load difference was proportional to the applied stress. The ratio of load differences can be expressed by dividing ΔL_x by ΔL_y in Eqs. (3a) and (3b) to obtain the numerical function of stress directionality and the conversion factor ratio:

$$p = \frac{\sigma_{res}^y}{\sigma_{res}^x} = \frac{\dfrac{\Delta L_x}{\Delta L_y} - \dfrac{\alpha_{//}}{\alpha_{\perp}}}{1 - \dfrac{\alpha_{//}\Delta L_x}{\alpha_{\perp}\Delta L_y}} \tag{4}$$

However, this model has the limitation that it requires the principal direction. The evaluation of each directional residual stresses by Knoop indentation is based on the assumption that the orientation of the Knoop indenter as a reference line is coincident with the principal direction.

Oppel [19] suggested that Knoop hardness is proportional to the magnitude of uniaxial stress and its direction relative to the indenter orientation. He also showed that hardness changes for 45-degree indenter orientation were equal to those for 135-degree orientation, which means that the sum of hardness changes for directions perpendicular to each other for a particular point at a particular loading is constant, and hardness changes do not depend on shear stresses. Using this previous research, we tried to analyze the relation among Knoop indentations along four directions in order to estimate the principal direction.

The basic concept of estimating principal direction by Knoop indentation begins from performing a Knoop indentation test four times along the 0-, 45-, 90- and 135-degree directions (Fig. 2). Any direction can be chosen as the 0-degree

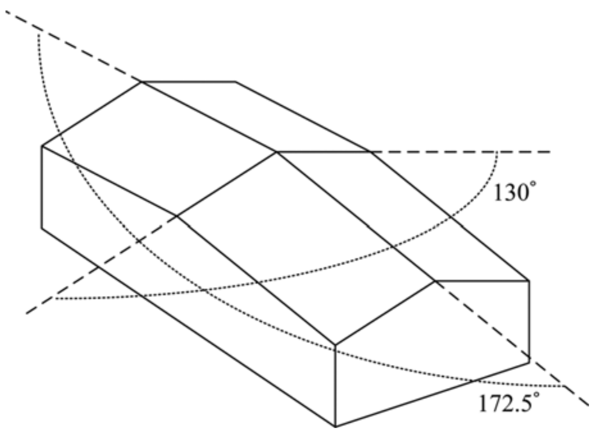

Fig. 1. Schematic diagram of Knoop indenter.

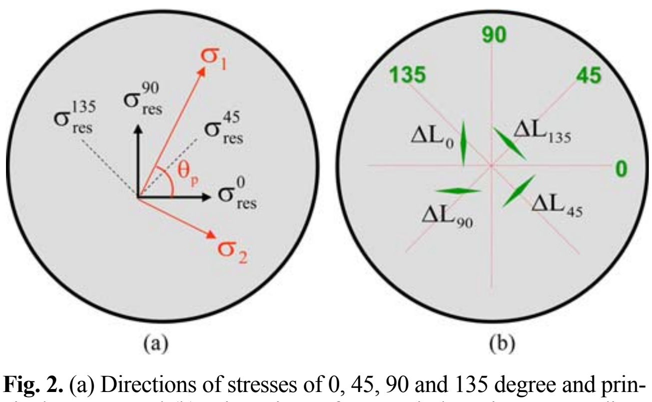

Fig. 2. (a) Directions of stresses of 0, 45, 90 and 135 degree and principal stresses and (b) orientations of Knoop indentations perpendicular to stress directions.

direction and the 45-, 90-, and 135 degree-directions determined from that. Each directional stress is defined as σ_{res}^{0}, σ_{res}^{45}, σ_{res}^{90} and σ_{res}^{135}, and the load differences generated by Knoop indentation along the defined four directions are also determined as ΔL_0, ΔL_{45}, ΔL_{90} and ΔL_{135}. When the stress state consists of two perpendicular stress components, we can evaluate the stress directionality p from the load differences measured by two Knoop indentations using previous work (Eqs. (3) and (4)). For four Knoop indentations, when σ_{res}^{0} and σ_{res}^{90}, and σ_{res}^{45} and σ_{res}^{135} are respectively perpendicular, the directionalities between σ_{res}^{0} and σ_{res}^{90} and between σ_{res}^{45} and σ_{res}^{135} can be determined by the ratio of ΔL_0 and ΔL_{90}, and the ratio of ΔL_{45} and ΔL_{135}. Here, p' and p'' are defined as

$$p' = \frac{\sigma_{res}^{90}}{\sigma_{res}^{0}} = \frac{\dfrac{\Delta L_0}{\Delta L_{90}} - \dfrac{\alpha_{//}}{\alpha_{\perp}}}{1 - \dfrac{\alpha_{//}}{\alpha_{\perp}}\dfrac{\Delta L_0}{\Delta L_{90}}}$$

$$p'' = \frac{\sigma_{res}^{135}}{\sigma_{res}^{45}} = \frac{\dfrac{\Delta L_{45}}{\Delta L_{135}} - \dfrac{\alpha_{//}}{\alpha_{\perp}}}{1 - \dfrac{\alpha_{//}}{\alpha_{\perp}}\dfrac{\Delta L_{45}}{\Delta L_{135}}} \tag{5}$$

In the plane stress transformation [17], σ_θ is determined by rotating the stress direction as:

$$\sigma_\theta = \frac{\sigma_x + \sigma_y}{2} + \frac{\sigma_x - \sigma_y}{2}\cos 2\theta + \tau_{xy}\sin 2\theta \tag{6}$$

$$\tan 2\theta_p = \frac{2\tau_{xy}}{\sigma_x - \sigma_y} \tag{7}$$

We can present the relation between angle of principal direction θ_p and the four directional stresses σ_{res}^{0}, σ_{res}^{45}, σ_{res}^{90} and σ_{res}^{135} using the equations as:

$$\sigma_\theta = \frac{\sigma_{res}^{0} + \sigma_{res}^{90}}{2} + \frac{\sigma_{res}^{0} - \sigma_{res}^{90}}{2}\cos 2\theta + \tau_{xy}\sin 2\theta \tag{8}$$

$$\tan 2\theta_p = \frac{2\tau_{xy}}{\sigma_{res}^{0} - \sigma_{res}^{90}} \tag{9}$$

τ_{xy} can be replaced with the normal stresses:

$$\sigma_\theta = \frac{\sigma_{res}^{0} + \sigma_{res}^{90}}{2} + \frac{\sigma_{res}^{0} - \sigma_{res}^{90}}{2}\cos 2\theta + \frac{\sigma_{res}^{0} - \sigma_{res}^{90}}{2}\sin 2\theta \cdot \tan 2\theta_p \tag{10}$$

when $\theta = 45^{\circ}$, cos 90 = 0 and sin 90 = 1, thus

$$\sigma_{res}^{45} = \frac{\sigma_{res}^{0} + \sigma_{res}^{90}}{2} + \frac{\sigma_{res}^{0} - \sigma_{res}^{90}}{2} \cdot \tan 2\theta_p \tag{11}$$

By dividing both sides by $\sigma_{res}^{0} + \sigma_{res}^{90}$, Eq. (11) becomes

$$\frac{\sigma_{res}^{45}}{\sigma_{res}^{0} + \sigma_{res}^{90}} = \frac{1}{2} + \frac{1}{2} + \frac{\sigma_{res}^{0} - \sigma_{res}^{90}}{\sigma_{res}^{0} + \sigma_{res}^{90}} \cdot \tan 2\theta_p \tag{12}$$

In Eq. (12), $\sigma_{res}^{0} + \sigma_{res}^{90}$ in the left term can be replaced by $\sigma_{res}^{45} + \sigma_{res}^{135}$, since the sum of normal stresses is constant (as discussed in Section 3 below):

$$\frac{\sigma_{res}^{45}}{\sigma_{res}^{45} + \sigma_{res}^{135}} = \frac{1}{2} + \frac{1}{2} + \frac{\sigma_{res}^{0} - \sigma_{res}^{90}}{\sigma_{res}^{0} + \sigma_{res}^{90}} \cdot \tan 2\theta_p \tag{13}$$

Eq. (13) is rearranged in terms of ratio of normal stress as:

$$\tan 2\theta_p = \frac{(1+p')(1-p'')}{(1-p')(1+p'')} \tag{14}$$

Here $p' = \dfrac{\sigma_{res}^{90}}{\sigma_{res}^{0}}$ and $p'' = \dfrac{\sigma_{res}^{135}}{\sigma_{res}^{45}}$, $\tan 2\theta_p$ can be expressed as functions of p' and p'', which can be evaluated from the results of Knoop experiments.

In addition, θ_p and θ_{p+90} are replaced with θ in Eq. (10), and then σ_{θ_p} and $\sigma_{\theta_{p+90}}$ become σ_1 and σ_2 as principal stresses:

$$\sigma_1 = \frac{\sigma_{res}^{0} + \sigma_{res}^{90}}{2} + \frac{\sigma_{res}^{0} - \sigma_{res}^{90}}{2}\cos 2\theta_p + \left(\frac{\sigma_{res}^{0} - \sigma_{res}^{90}}{2}\right)\sin 2\theta_p \cdot \tan 2\theta_p \tag{15}$$

$$\sigma_2 = \frac{\sigma_{res}^{0} + \sigma_{res}^{90}}{2} + \frac{\sigma_{res}^{0} - \sigma_{res}^{90}}{2}\cos 2\theta_p - \left(\frac{\sigma_{res}^{0} - \sigma_{res}^{90}}{2}\right)\sin 2\theta_p \cdot \tan 2\theta_p \tag{16}$$

The ratio of σ_1 and σ_2 can be expressed from Eqs. (15) and (16) as:

$$\frac{\sigma_2}{\sigma_1} = \frac{\left(1 + \dfrac{\sigma_{res}^{90}}{\sigma_{res}^{0}}\right)\cos 2\theta_p - \left(1 - \dfrac{\sigma_{res}^{90}}{\sigma_{res}^{0}}\right)}{\left(1 + \dfrac{\sigma_{res}^{90}}{\sigma_{res}^{0}}\right)\cos 2\theta_p + \left(1 - \dfrac{\sigma_{res}^{90}}{\sigma_{res}^{0}}\right)} \tag{17}$$

Finally, $p' = \dfrac{\sigma_{res}^{90}}{\sigma_{res}^{0}}$ is applied to Eq. (17) and the ratio of principal stresses can be expressed as functions of p' and θ_p:

$$\frac{\sigma_2}{\sigma_1} = \frac{(1+p')\cos 2\theta_p - (1-p')}{(1+p')\cos 2\theta_p + (1-p')} \tag{18}$$

3. EXPERIMENTAL PROCEDURES

Instrumented indentation tests were carried out using an AIS 3000 system (Frontics, Inc.). The resolutions of load and displacement are 5.6 gf and 0.1 μm, respectively. The Knoop indenter with diamond tip was produced by Synton MDP (Switzerland) (Fig. 3). Machine compliance is calculated with standard hardness blocks.

A stress-generating jig with two independent orthogonal loading axes was designed in order to strain the rectangular beam and cruciform specimens (Fig. 4) [14]. The applied biaxial surface strains were converted to biaxial stresses of

Fig. 3. AIS 3000 system by Frontics, Inc. and Knoop indenter produced by Synton MDP.

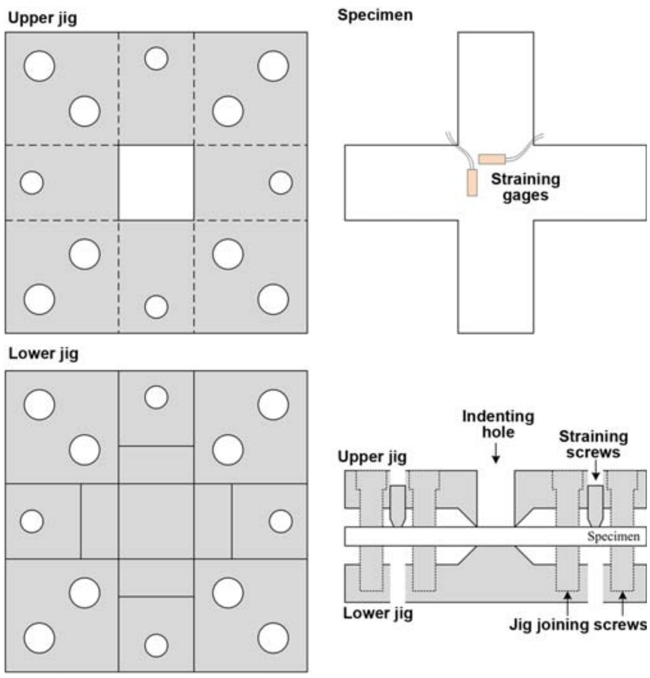

Fig. 4. Schematic diagram of Stress-generating jig with two independent orthogonal loading axes.

the two orthogonal axes using the Young's modulus and Poisson's ratio of the specimens. To keep the applied stress below the elastic limit, the difference of the two orthogonal principal stress components was maintained below the specimen yield strength according to the Tresca yield criterion.

We prepared API X65 steels specimens, which are used in such industrial facilities as pipes and tanks. The materials have elastic modulus 180 GPa and yield strengths 466 MPa at room temperature respectively. The 15-mm-thick cruciform specimens were machined from a thick plate and heat treated to remove internal stress. The specimen surfaces were mechanically polished for the subsequent indentation tests.

4. RESULTS AND DISCUSSION

To measure the principal direction of the residual stresses, we applied x-directional stress of 198 MPa and y-directional stress of 103 MPa using the stress-generating jig. In this experiment, 30° of principal direction was pre-determined as the standard (0 degree) line. Fig. 5 shows a schematic view of the directions of applied stress and Knoop indentations. ΔL_0, ΔL_{45}, ΔL_{90} and ΔL_{135} were measured from Knoop indentations along each direction and unstressed sample. We intended to make four Knoop indentations in small area as shown in Fig. 6, which is because target area could be small in case of in-filed application although residual stress is uniform in center of cruciform sample in this study.

Also, we estimated plastic zone in four Knoop indentations with Gao's studies [18] based on modified expanding cavity model as following equation:

$$\left(\frac{r_c}{a}\right)^3 = \frac{1}{3}\frac{E}{\sigma_y}\cot\alpha \tag{19}$$

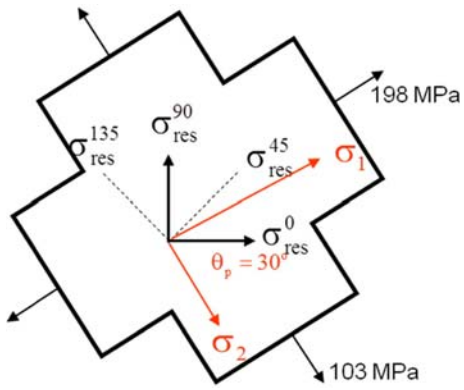

Fig. 5. Schematic view of the directions of applied stress and Knoop indentations.

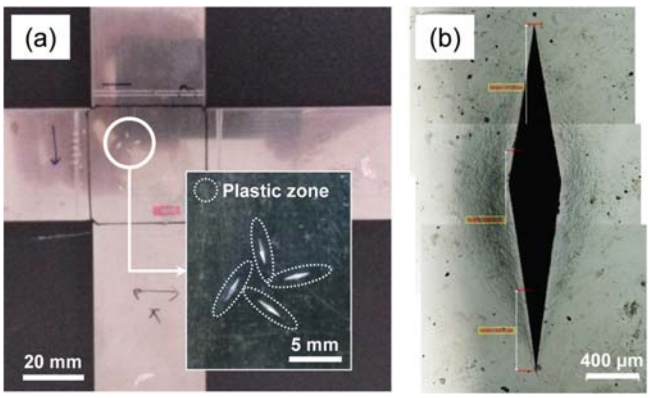

Fig. 6. (a) Locations of four Knoop indentations and estimated plastic zone size indicated by dotted lines and (b) enlarged optical image of residual Knoop indentation mark.

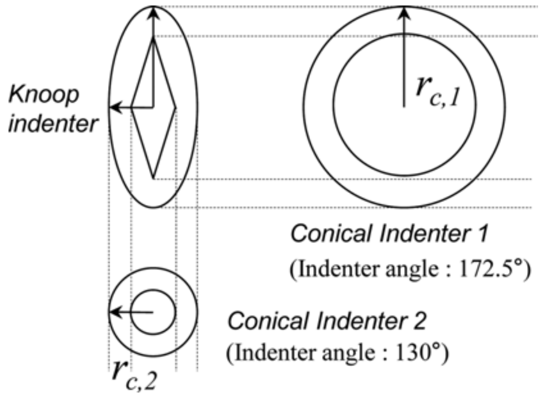

Fig. 7. Anisotropic plastic zone size beneath Knoop indentation estimated by those of two conical indentations corresponding to long and short diagonals of Knoop indenter.

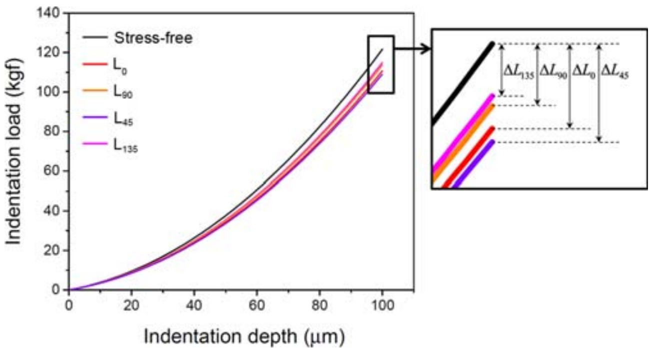

Fig. 8. Indentation load-depth curves measured along with direction of 0, 45, 90 and 135 degree from pre-determined standard line that is direction of 0 degree.

where r_c is the radius of plastic zone, a and α are the contact radius and the indenter half angle, respectively. We assumed Knoop indenter as two conical indenters as in Fig. 7 along long and short diagonals. For indentation depth of 100 μm, radii of plastic zone are 3146 and 840 μm using Eq. (19), respectively, which are illustrated as white dotted line in Fig. 6. With Gao's model, we confirmed plastic zone of four Knoop indentations were not overlapped one another. This estimation is just based on theoretical ECM model, and plastic zone of a long diagonal of Knoop indenter is expected to be smaller, since pile-up at the edges of long diagonal is hardly occurred in real image of a Knoop indent as Fig. 6(b). Geometrical shape of Knoop indenter is seemed to induce plastic flow beneath the indenter was concentrated along the short diagonal.

Figure 8 shows the load difference between each directional load-depth curve. Four load differences are different one another, which means effects of residual stress on Knoop indentation are different along with direction because of anisotropic shape of the indenter. In this case (Fig. 8), Knoop indentation showed the highest dependence with biaxial residual stress at 45° direction and the lowest at 135°. From the load differences at the maximum indentation depth, p',

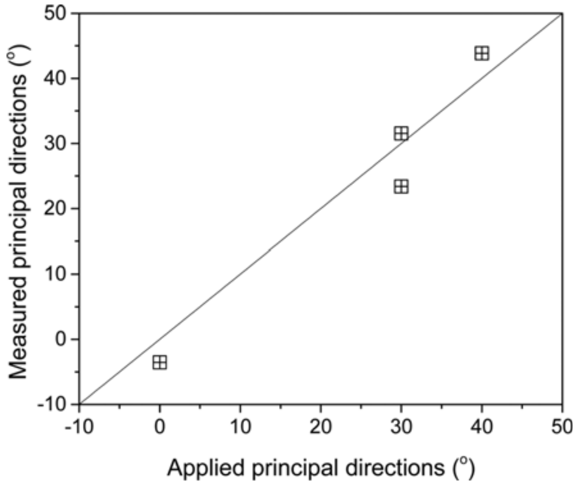

Fig. 9. Comparison of measured and applied principal directions of biaxial residual stress on cruciform sample.

p'' and θ_p were determined using Eqs. (5) and (14). The principal direction θ_p is 28.8°, in good agreement with the pre-determined angle of 30°. Additional results showing relationship between measured and applied principal directions for 0, 30, and 40° are shown in Fig. 9, which shows good agreement. Deviations range from 5 to 20%, and average deviation is about 10%.

We also tried to verify the assumption made in deriving the model that the sum of normal stresses is constant. Since $\sigma_{res}^{0}+\sigma_{res}^{90} = \sigma_{res}^{45}+\sigma_{res}^{135}$, $\Delta L_0 + \Delta L_{90}$ should be also equal to $\Delta L_{45} + \Delta L_{135}$:

$$\Delta L_0 + \Delta L_{90} = \Delta L_{45} + \Delta L_{135}\,. \tag{20}$$

The summary of each sum of load differences in Fig. 10 shows that this assumption is reasonable. The sums are averaged from reproducible 2~3 indentation load-depth data sets (four load-depth data per one set) and their standard deviations are also presented in Fig. 10. Testing area of cruciform samples is limited due to stress-generating jig, which allowed maximum 3 data sets except strain gage site. The stress-free and stressed indentation load-depth curves are representative data from each data set and also show that Knoop indentation is capable to detect different biaxial stress state and principal direction. Thus, for example, another value of ΔL_{135} can be estimated from the three values of ΔL_0, ΔL_{45} and ΔL_{90}, showing that three repetitions of Knoop indentation can determine principal direction and stress directionality p, instead of four repetitions, it is summarized in Eq. (21).

$$\begin{pmatrix} \Delta L_0 \\ \Delta L_{90} \\ \Delta L_{45} \\ \Delta L_{135} \end{pmatrix} = \begin{pmatrix} 0 & -1 & 1 & 1 \\ -1 & 0 & 1 & 1 \\ 1 & 1 & 0 & -1 \\ 1 & 1 & -1 & 0 \end{pmatrix} \begin{pmatrix} \Delta L_0 \\ \Delta L_{90} \\ \Delta L_{45} \\ \Delta L_{135} \end{pmatrix} \tag{21}$$

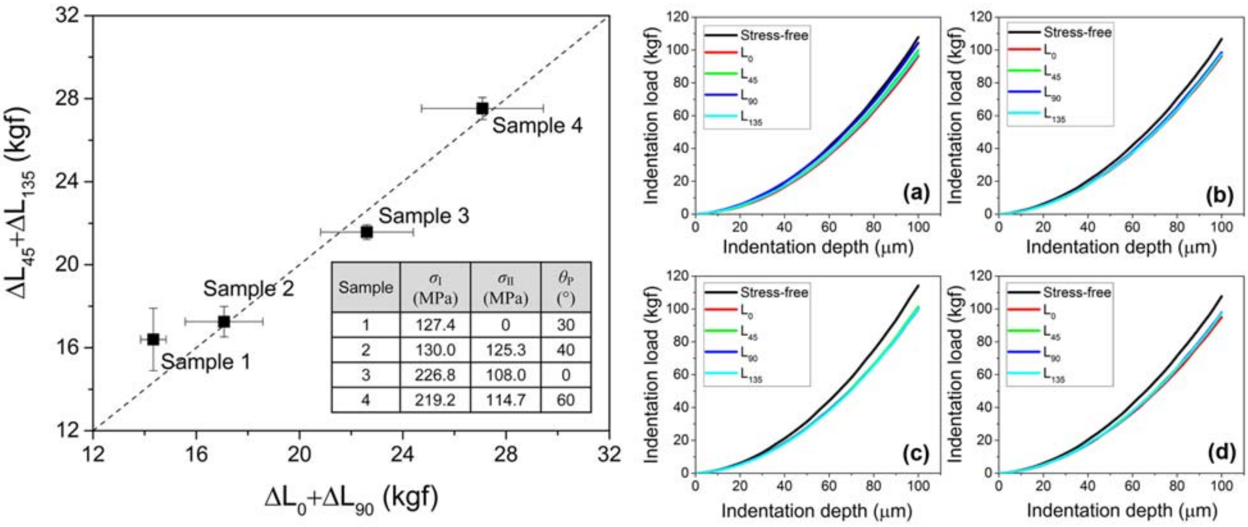

Sample	σ_I (MPa)	σ_{II} (MPa)	θ_P (°)
1	127.4	0	30
2	130.0	125.3	40
3	226.8	108.0	0
4	219.2	114.7	60

Fig. 10. Comparison of sum of load differences: $\Delta L_0 + \Delta L_{90}$ and $\Delta L_{45} + \Delta L_{135}$. (a) Sample 1, (b) Sample 2, (c) Sample 3, and (d) Sample 4.

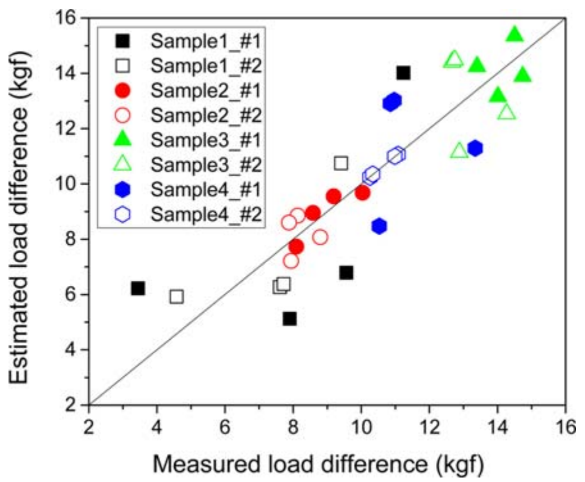

Fig. 11. Load difference estimated by other three load differences evaluated by using Eq. (21).

Based on Eq. (21), load differences at each direction shown in Fig. 11 are estimated for other three ΔL. Two data sets are included in one sample, so that 8 load differences are estimated and they show good agreement with experimental results. This approach would be applicable on curved surface in operating facilities such as pipeline and pressure vessel, and confirmation of one questionable Knoop indentation load-depth curve, which might have artificial error.

5. CONCLUSION

We proposed a Knoop indentation model to estimate the principal direction of residual stresses. Four indentation tests were performed along the 0-, 45-, 90- and 135-degree directions from an arbitrary standard line. From previous research on determining stress directionality, the principal direction and ratio of principal stress were derived theoretically in terms of ratio of load differences. Verification experiments were done to compare the pre-determined direction with the estimated principal direction; these values showed good agreement.

ACKNOWLEDGEMENTS

This research was supported by Basic Science Research Program through the National Research Foundation of Korea (NRF) funded by the Ministry of Education, Science and Technology (2013R1A1A2063474), and by Basic Science Research Program through the National Research Foundation of Korea (NRF) funded by the Ministry of Education (2014R1A1A2058799).

REFERENCE

1. E.-C. Jeon, J.-Y. Kim, M.-K. Baik, S.-H. Kim, J.-S. Park, and D. Kwon, *Mat. Sci. Eng. A-Struct.* **419**, 196 (2006).
2. J.-Y. Kim, S.-H Kim, J.-S Lee, K.-W Lee, and D. Kwon, *Met. Mater. Int.* **12**, 219 (2006).
3. Y.-C. Kim, S.-K. Kang, J.-Y. Kim, and D. Kwon, *J. Mater. Sci.* **48**, 232 (2013).
4. Y.-H Lee, Y. Kim, Y.-C. Kim, J.-Y. Kim, J.-I. Jang, *Met. Mater. Int.* **20**, 439 (2014).
5. Y.-H. Lee, S.-M. Ahn, J.-Y. Kim, C.-P. Park, and H.-K. Jang, *Korean J. Met. Mater.* **53**, 162 (2015).
6. T. Y. Tsui, W. C. Oliver, and G. M. Pharr, *J. Mater. Res.* **11**, 752 (1996).
7. A. Bolshakov, W. C. Oliver, and G. M. Pharr, *J. Mater. Res.* **11**, 760 (1996).
8. S. Suresh and A. E. Giannakopoulos, *Acta Mater.* **46**, 5755 (1998).
9. S. Carlsson and P. L. Larsson, *Acta Mater.* **49**, 2179 (2001).
10. S. Carlsson and P. L. Larsson, *Acta Mater.* **49**, 2193 (2001).

11. J. G. Swadener, B. Taljat, and G. M. Pharr, *J. Mater. Res.* **16**, 2091 (2001).
12. A. E. Giannakopoulos, *J. Appl. Mech.* **70**, 638 (2003).
13. Y.-H. Lee and D. Kwon, *Scripta Mater.* **49**, 459 (2003).
14. Y.-H. Lee and D. Kwon, *Acta Mater.* **52**, 1555 (2004).
15. K. Zeng, A. E. Giannakopoulos, D. Rowcliffe, and P. Meier, *J. Am. Ceram. Soc.* **81**, 689 (1998).
16. M.-J. Choi, S.-K. Kang, I. Kang, and D. Kwon, *J. Mater. Res.* **1** (2011).
17. G. E. Dieter, *Mechanical Metallurgy*, McGraw-Hill, New York (1986).
18. X.-L. Gao, X. N. Jing, and G. Subhash, *Int. J. Solids Struct.* **43**, 2193 (2006).
19. G. U. Oppel, *Exp. Mech.* **4**, 135 (1964).